Weak antilocalization in two-dimensional systems with large Rashba splitting

L. E. Golub,[1] I. V. Gornyi,[1,2] and V. Yu. Kachorovskii[1]
[1]*Ioffe Institute, St. Petersburg 194021, Russia*
[2]*Institut für Nanotechnologie, Karlsruhe Institute of Technology, 76021 Karlsruhe, Germany*
(Received 5 April 2016; published 20 June 2016)

We develop the theory of quantum transport and magnetoconductivity for two-dimensional electrons with an arbitrarily large (even exceeding the Fermi energy), linear-in-momentum Rashba or Dresselhaus spin-orbit splitting. For short-range disorder potentials, we derive the analytical expression for the quantum conductivity correction, which accounts for interference processes with an arbitrary number of scattering events and is valid beyond the diffusion approximation. We demonstrate that the zero-field conductivity correction is given by the sum of the universal logarithmic "diffusive" term and a "ballistic" term. The latter is temperature independent and encodes information about the spectrum properties. This information can be extracted experimentally by measuring the conductivity correction at different temperatures and electron concentrations. We calculate the quantum correction in the whole range of classically weak magnetic fields and find that the magnetoconductivity is negative both in the diffusive and in the ballistic regimes, for an arbitrary relation between the Fermi energy and the spin-orbit splitting. We also demonstrate that the magnetoconductivity changes with the Fermi energy when the Fermi level is above the "Dirac point" and does not depend on the Fermi energy when it goes below this point.

DOI: 10.1103/PhysRevB.93.245306

I. INTRODUCTION

Weak localization is a coherent phenomenon in the low-temperature transport in disordered systems. Transport in such systems is realized by various trajectories, including a special class of trajectories with closed loops. The underlying physics of the weak localization is the enhancement of the backscattering amplitude which results from the constructive interference of the waves propagating along the loops in opposite directions (clockwise and counterclockwise). Since interference increases the backscattering amplitude, the quantum conductivity correction is negative and is proportional to the ratio of the de Broglie wavelength to the mean free path [1]. Remarkably, this correction diverges logarithmically at low temperatures in the two-dimensional (2D) case. Such a divergence is a precursor of strong localization and reflects universal symmetry properties of the system.

Dephasing processes suppress interference and, consequently, strongly affect the conductivity correction. Specifically, the typical size of the interfering paths is limited by the time of electron dephasing, τ_ϕ. At low temperatures, the dephasing rate is dominated by inelastic electron-electron collisions. The phase space for such collisions decreases with lowering temperature. Therefore, one can probe dephasing processes by measuring the temperature dependence of conductivity in the weak-localization regime [2]. Another possibility to affect the interference-induced quantum correction to the conductivity is the application of magnetic field. The Aharonov-Bohm effect introduces a phase difference for the waves traveling along the closed loop in opposite directions. This phase difference is equal to a double magnetic flux passing through the loop. The anomalous magnetoconductivity allows one to extract the dephasing time even more accurately than the temperature measurements since the low-field magnetoconductivity is not masked by other effects [1,3].

Since weak localization is caused by the interference of paths related to each other by time inversion, it is extremely sensitive to the spin properties of the interfering particles. In systems with spin-orbit coupling (see Fig. 1), an additional spin-dependent phase is acquired by electrons passing the loops clockwise and anticlockwise. As a result, the interference depends on the electron spin states before and after passing the loop. Importantly, in the presence of spin-orbit coupling, the interference becomes destructive, resulting in a positive correction to the conductivity. This interference effect is called weak antilocalization. The magnetic field suppresses this correction, making the conductivity smaller than in the zero field, i.e., the magnetoconductivity is negative [1].

The theory of weak localization developed in the 1980's for diffusive systems allowed one to explain a number of experimental data in various metallic and semiconductor structures [2]. The spin-orbit interaction has been treated as spin relaxation, which adds an additional channel for dephasing of the triplet contributions to the quantum corrections [1]. However, this approach is insufficient for 2D semiconductor heterostructures with the linear-in-momentum spin-orbit splitting of the spectrum. A relevant theory of weak localization was developed in the mid-1990's [4]. It describes very well the experimental data [5,6].

With increasing the magnetic field, the magnetic length l_B becomes smaller than the mean free path l. This regime of weak localization cannot be treated within the model of a diffusive electron motion along large scattering paths. By contrast, the main contribution to the interference correction comes from short ballistic trajectories with a few scattering events [7–9]. Experimentally, the ballistic regime can be more easily achieved in high-quality heterostructures with high electron mobility. The point is that in such structures, the interval of fields, where $l_B < l$ but at the same time the magnetic field is classically weak, can be very wide.

Positive magnetoconductivity due to weak localization in the ballistic regime was calculated in Refs. [7,9]. In the presence of a moderate spin-orbit splitting of the spectrum, the "ballistic" magnetoconductivity was obtained in

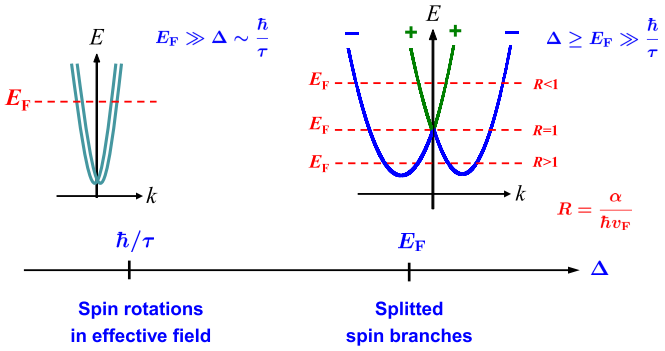

FIG. 1. Electron spectrum and regimes of spin dynamics depending on the strength of the Rashba splitting. Left: Regime of spin rotations in the effective magnetic field realized at moderate spin-orbit splitting $\Delta \sim \hbar/\tau$; the weak-localization theory is developed in Ref. [12]. Right: Regime of well-separated spin branches at strong spin-orbit splitting ($\Delta \sim E_F$) considered in the present work.

Refs. [10–12]. These results were used to fit the weak-localization [13] and weak-antilocalization [12,14] data in various high-mobility heterostructures.

In Refs. [10–12], the spin-orbit splitting was assumed to be comparable to or even larger than the momentum scattering rate $\hbar/\tau$ (see Fig. 1). In this case, the spin dynamics can be well described by electron spin rotations in the effective momentum-dependent magnetic field [15,16]. However, when the spin-orbit splitting becomes of the order of the Fermi energy, the effects of spin-orbit interaction on the electron orbital motion cannot be neglected in the calculation of the conductivity correction.

Recently, 2D systems have become available where such an ultrastrong splitting can be realized. Examples are electrons near the surface of polar semiconductors and at $LaAlO_3/SrTiO_3$ interfaces, or holes in HgTe-based quantum well structures with a large spin-orbit splitting [17–19]. In such systems, the spin energy branches are well separated (see Fig. 1, right panel), which results in a strongly coupled dynamics of electron spin and orbital degrees of freedom. The classical conductivity in such systems was analyzed in Ref. [20]. Weak localization for well-separated spin branches was considered in Refs. [21,22] in the diffusive regime and in zero magnetic field only. Recently, weak localization in spin-orbit metals based on HgTe quantum wells has been examined in the model of doubly degenerate branches of the massive Dirac fermions [23–27].

In the present work, we develop a theory of weak localization for systems with an arbitrarily large splitting of the spin branches. We study the quantum interference in the presence of a short-range disorder potential which provides efficient interbranch scattering. We consider contributions to the anomalous magnetoconductivity from an arbitrary number of scatterers and derive a general expression for the magnetoconductivity valid in both diffusion and ballistic regimes of weak localization.

The paper is organized as follows. In Sec. II, we formulate the model. In Sec. III, we present the derivation of the interference-induced conductivity correction. In Sec. IV, the results for the magnetoconductivity and the zero-field correction are presented and discussed. Section V summarizes our conclusions.

II. MODEL

The Hamiltonian of 2D electrons has the form

$$H = \frac{\hbar^2 k^2}{2m} + \alpha(\boldsymbol{\sigma} \times \boldsymbol{k})_z, \tag{1}$$

where $\boldsymbol{k}$ is a 2D momentum, z is a normal to the structure, m is the effective mass, $\boldsymbol{\sigma}$ is a vector of Pauli matrices, and α is the Rashba constant. The isotropic energy spectrum consists of two branches labeled by the index $s = \pm$,

$$E_s(k) = \frac{\hbar^2 k^2}{2m} + s\alpha k, \tag{2}$$

with the splitting $\Delta = 2\alpha k$ (Fig. 1). It is worth noting that the same spectrum describes electrons with a $\boldsymbol{k}$-linear isotropic 2D Dresselhaus spin-orbit interaction [16,28] with the substitution of α by the 2D Dresselhaus constant. The eigenfunctions in the two branches are spinors,

$$|\boldsymbol{k}, s\rangle = e^{i\boldsymbol{k}\cdot\boldsymbol{r}} \frac{1}{\sqrt{2}} \begin{pmatrix} 1 \\ -is e^{i\varphi_{\boldsymbol{k}}} \end{pmatrix}, \tag{3}$$

where $\varphi_{\boldsymbol{k}}$ is the polar angle of $\boldsymbol{k}$.

The spectrum (2) is approximately linear in the vicinity of $k = 0$, where the $\pm$ bands touch each other (see Fig. 1, right panel). In what follows, we will term this special point the "Dirac point." We will first consider the situation when the Fermi energy is located above the Dirac point. In this case, the eigenstates at the Fermi level belong to two different branches, and Fermi wave vectors $k_F^{\pm}$ are different:

$$k_F^{\pm} = \frac{m}{\hbar}\left(v_F \mp \frac{\alpha}{\hbar}\right). \tag{4}$$

Here,

$$v_F = \sqrt{2E_F/m + \alpha^2/\hbar^2} \tag{5}$$

is the Fermi velocity equal in both branches and E_F is the Fermi energy counted from the Dirac point.

Disorder leads to the following types of scattering processes: intrabranch (++ and −−) and interbranch (+− and −+). In this paper we consider the short-range Gaussian disorder,

$$\overline{V(\boldsymbol{r})V(\boldsymbol{r}')} = V_0^2 \delta(\boldsymbol{r} - \boldsymbol{r}').$$

Here, $\overline{\cdots}$ stands for averaging over disorder realizations, and V_0 quantifies the strength of the scattering potential. The scattering matrix element between the states $s,\boldsymbol{k}$ and $s',\boldsymbol{k}'$ is given by

$$\langle \boldsymbol{k}' s' | V | \boldsymbol{k} s \rangle = A_{\boldsymbol{k}'\boldsymbol{k}} V_{s's}, \tag{6}$$

where $A_{\boldsymbol{k}'\boldsymbol{k}} = \int V(\boldsymbol{r}) e^{i(\boldsymbol{k}-\boldsymbol{k}')\mathbf{r}} d\boldsymbol{r}/V_0$,

$$V_{s's} = V_0(1 + ss' e^{-i\theta})/2,$$

and $\theta = \varphi_{\boldsymbol{k}'} - \varphi_{\boldsymbol{k}}$ is the scattering angle. Importantly, the short-range potential provides effective interbranch scattering for an

arbitrary spin-orbit splitting. The total (quantum) disorder-averaged scattering rate is the same in both branches:

$$\frac{1}{\tau} = \frac{2\pi}{\hbar}\langle |V_{++}|^2 g_+ + |V_{+-}|^2 g_- \rangle_\theta = \frac{m}{\hbar^3} V_0^2. \tag{7}$$

Here, the angular brackets denote averaging over θ, and the densities of states at the Fermi energy in the branches are given by

$$g_\pm = \frac{m}{2\pi\hbar^2}(1 \mp R). \tag{8}$$

The parameter R is introduced according to

$$R = \frac{\alpha}{\hbar v_F}. \tag{9}$$

As shown in Appendix A (see also Ref. [20]), the classical Drude conductivity is given by

$$\sigma_D = e^2 v_F^2 \tau \frac{m}{2\pi\hbar^2}(1 + R^2) = \frac{ne^2\tau}{m}, \tag{10}$$

where the 2D electron concentration is

$$n = \frac{m^2 v_F^2}{2\pi\hbar^2}(1 + R^2). \tag{11}$$

When the Fermi energy is located below the Dirac point ($R > 1$), the Fermi contour also consists of two concentric circles, "1" and "2," but they both belong to the outer spin branch $s = -$ (Fig. 1). The Fermi wave vectors $k_F^{(1,2)}$ are substantially different, while the Fermi velocities in the branches are equal in this case as well. The densities of states are given by

$$g^{(1,2)} = \frac{m}{2\pi\hbar^2}(R \pm 1), \tag{12}$$

and the concentration is given by Eq. (11) as well.

III. CONDUCTIVITY CALCULATION

The quantum correction to the conductivity in systems with spin-orbit interaction can be calculated by two approaches. The first one uses the basis of electron states with definite spin projections on the z axis, $\uparrow$ and $\downarrow$. In this approach, the conductivity correction is presented as a result of interference of electronic waves with a definite total angular momentum: The interference amplitude, cooperon, is a sum of contributions from the singlet and triplet states [4,10–12,29,30]. An alternative approach uses the basis of chiral states (3). This approach has been used for calculations of the conductivity correction in zero magnetic field and, recently, for calculations of its magnetic field dependence in HgTe quantum wells [21,22,25–27]. In the present work we use both approaches and demonstrate that they lead to the same results. In this section we derive the conductivity correction working in the basis of singlet and triplet states. In Appendix B and the Supplemental Material [31], we derive the correction in the basis of chiral states.

We investigate the two cases when the Fermi level is above and below the Dirac point (Fig. 1). We start with the first case, corresponding to $R < 1$.

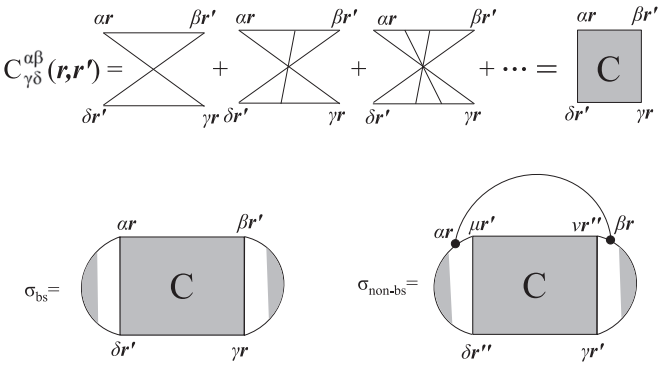

FIG. 2. Diagrammatic cooperon equation and conductivity corrections.

A. Fermi level above the Dirac point

The retarded (R) and advanced (A) Green's functions in the subband s are given by

$$G_s^{R,A}(\boldsymbol{r},\boldsymbol{r}') = G_0^{R,A}(\boldsymbol{r},\boldsymbol{r}';k_F^s)\frac{1}{2}\begin{pmatrix} 1 & \pm ise^{-i\phi} \\ \mp ise^{i\phi} & 1 \end{pmatrix}. \tag{13}$$

Here, ϕ is the polar angle of the vector $\boldsymbol{\rho} = \boldsymbol{r} - \boldsymbol{r}'$, k_F^s are the wave vectors at the Fermi level in two subbands, Eq. (4), and $G_0^{R,A}(\boldsymbol{r},\boldsymbol{r}';k_F)$ is the standard Green's function in a simple parabolic band with the Fermi wave vector k_F:

$$G_0^{R,A}(\boldsymbol{r},\boldsymbol{r}';k_F) = \mp i\frac{\sqrt{k_F}}{\hbar v_F\sqrt{2\pi\rho}} \times \exp\left[\pm k_F\rho - \frac{\rho}{2l} \mp i\frac{\pi}{4} + \frac{i}{2}\Phi(\boldsymbol{r},\boldsymbol{r}')\right], \tag{14}$$

with $l = v_F\tau$. The magnetic-field-induced phase is

$$\Phi(\boldsymbol{r},\boldsymbol{r}') = (y + y')(x' - x)/l_B^2, \tag{15}$$

where

$$l_B = \sqrt{\hbar/|eB|}$$

is the magnetic length for elementary charge ($e < 0$). Here, we used the fact that τ and l are the same in both branches.

The interference-induced correction to the conductivity is expressed via the cooperon (see Fig. 2). In the basis of states with spin projections on the z axis, $\alpha,\beta,\gamma,\delta = \uparrow,\downarrow$, the cooperon satisfies the following equation:

$$\mathcal{C}^{\alpha\beta}_{\gamma\delta}(\boldsymbol{r}_1,\boldsymbol{r}_2) = V_0^2 P^{\alpha\beta}_{\gamma\delta}(\boldsymbol{r}_1,\boldsymbol{r}_2) + \int d\boldsymbol{r}\, P^{\alpha\mu}_{\gamma\nu}(\boldsymbol{r}_1,\boldsymbol{r})\mathcal{C}^{\mu\beta}_{\nu\delta}(\boldsymbol{r},\boldsymbol{r}_2), \tag{16}$$

where

$$P^{\alpha\mu}_{\gamma\nu}(\boldsymbol{r}_1,\boldsymbol{r}) = V_0^2 G^R_{\alpha\mu}(\boldsymbol{r}_1,\boldsymbol{r})G^A_{\gamma\nu}(\boldsymbol{r}_1,\boldsymbol{r}),$$

and $G^{R,A}_{\alpha\mu} = \sum_s (G^{R,A}_s)_{\alpha\mu}$.

Under the condition of well-separated spin branches, $|k_F^+ - k_F^-|l \gg 1$, which we assume from now on, the product $G_s^R(\boldsymbol{r}_1,\boldsymbol{r})G_{s'}^A(\boldsymbol{r}_1,\boldsymbol{r})$ oscillates rapidly on the scale of the mean free path if $s \neq s'$. Therefore, $\hat{P}$ has only two terms in the sum

with $s = s'$:

$$P^{\alpha\mu}_{\gamma\nu}(\boldsymbol{r}_1,\boldsymbol{r}) = V_0^2 \sum_{s=\pm} \left(G^R_s\right)_{\alpha\mu}\left(G^A_s\right)_{\gamma\nu}. \tag{17}$$

Summation over s yields the 16 components of the matrix $\hat{P}$. Passing to the basis of states with a fixed total angular momentum and its projection to the z axis, i.e., to the basis $\uparrow\uparrow$,$(\uparrow\downarrow + \downarrow\uparrow)/\sqrt{2}$,$(\uparrow\downarrow - \downarrow\uparrow)/\sqrt{2}$, $\downarrow\downarrow$, we obtain that the triplet state with the zero momentum projection, i.e., $(\uparrow\downarrow + \downarrow\uparrow)/\sqrt{2}$, does not contribute to weak localization. The matrix $\hat{P}$ corresponding to the three other states, $\uparrow\uparrow$,$(\uparrow\downarrow - \downarrow\uparrow)/\sqrt{2}$, $\downarrow\downarrow$, has the following form:

$$\hat{P} = P_0 \begin{pmatrix} \frac{1}{2} & -i\frac{R}{\sqrt{2}}e^{-i\phi} & \frac{1}{2}e^{-2i\phi} \\ i\frac{R}{\sqrt{2}}e^{i\phi} & 1 & i\frac{R}{\sqrt{2}}e^{-i\phi} \\ \frac{1}{2}e^{2i\phi} & -i\frac{R}{\sqrt{2}}e^{-i\phi} & \frac{1}{2} \end{pmatrix}, \tag{18}$$

where

$$P_0(\boldsymbol{r},\boldsymbol{r}') = \frac{\exp\left(-|\boldsymbol{r}-\boldsymbol{r}'|/\tilde{l}\right)}{2\pi l|\boldsymbol{r}-\boldsymbol{r}'|} e^{i\Phi(\boldsymbol{r},\boldsymbol{r}')}, \tag{19}$$

with $\tilde{l} = l/(1+\tau/\tau_\phi)$, and $\Phi(\boldsymbol{r},\boldsymbol{r}')$ given by Eq. (15).

It is worth comparing the form of the matrix $\hat{P}$, Eq. (18), with its form for weakly split Fermi circles at $\Delta \ll E_F$ ($R \to 0$). In that case, the matrix $\hat{P}$ had the form of a 4×4 block-diagonal matrix with a separate triplet 3×3 block and an independent singlet sector. In the limit $\Delta\tau/\hbar \to \infty$ (but still $R = 0$) the triplet state with zero spin projection decouples and its matrix elements vanish, so that the triplet block becomes a 2×2 matrix [11]. However, Eq. (18) demonstrates that, for strongly split spin branches ($R \neq 0$), the singlet cooperon state becomes mixed with the two triplet ones. This mixing, linear in the parameter R, arises due to the difference in the densities of states in the spin branches: $g_+ - g_- \propto R$, Eq. (8).

The cooperon can be found in the basis of Landau level states with charge $2e$, $\Psi_{Nq}(\boldsymbol{r})$:

$$\mathcal{C}^{\alpha\beta}_{\gamma\delta}(\boldsymbol{r},\boldsymbol{r}') = \sum_{N,N',q,q'} \mathcal{C}^{\alpha\beta}_{\gamma\delta}(N,N')\Psi^*_{Nq}(\boldsymbol{r})\Psi_{N'q'}(\boldsymbol{r}'),$$

where $N = 0,1,2,\ldots$ is the Landau level number, and q is the in-plane wave vector for the Landau gauge. Expanding the matrix $\hat{P}$, Eq. (18), over this basis, we obtain from Eq. (16) an infinite system of linear equations for the coefficients $\mathcal{C}^{\alpha\beta}_{\gamma\delta}(N,N')$. It can be block-diagonalized in the basis of states with fixed $N + s_z$, where $s_z = 1,-1$ is the angular momentum projection in the triplet state while $s_z = 0$ describes the singlet. The equation for the blocks $\mathcal{C}(N)$ has the following form,

$$\mathcal{C}(N) = V_0^2 A_N + A_N \mathcal{C}(N), \tag{20}$$

where

$$A_N = \begin{pmatrix} \frac{1}{2}P_{N-2} & i\frac{R}{\sqrt{2}}P^{(1)}_{N-2} & \frac{1}{2}P^{(2)}_{N-2} \\ i\frac{R}{\sqrt{2}}P^{(1)}_{N-2} & P_{N-1} & -i\frac{R}{\sqrt{2}}P^{(1)}_{N-1} \\ \frac{1}{2}P^{(2)}_{N-2} & -i\frac{R}{\sqrt{2}}P^{(1)}_{N-1} & \frac{1}{2}P_N \end{pmatrix}. \tag{21}$$

Here, $P^{(m)}_N$ ($m = 1,2$) and $P_N \equiv P^{(0)}_N$ are defined as follows,

$$P^{(m)}_N = \frac{l_B}{l}\sqrt{\frac{N!}{(N+m)!}} \times \int_0^\infty dx \exp(-xl_B/\tilde{l} - x^2/2)x^m L^m_N(x^2), \tag{22}$$

with L^m_N being the Laguerre polynomials. All values with negative indexes should be substituted by zeros.

The conductivity correction is a sum of two contributions shown in Fig. 2:

$$\sigma = \sigma_{\rm bs} + \sigma_{\rm non\text{-}bs}.$$

The backscattering contribution to the magnetoconductivity is given by

$$\sigma_{\rm bs} = \frac{\hbar}{4\pi}\int d\boldsymbol{r}\int d\boldsymbol{r}' \sum_{\alpha\beta}[\tilde{\mathcal{C}}(\boldsymbol{r},\boldsymbol{r}')\Gamma(\boldsymbol{r},\boldsymbol{r}')]^{\alpha\beta}_{\beta\alpha}, \tag{23}$$

where $\tilde{\mathcal{C}} = \mathcal{C} - V_0^2 P$ is the cooperon calculated starting from three scattering lines. The squared electric current vertex is presented by the following operator,

$$\Gamma = \sum_{s=\pm}\left(\frac{iel}{\hbar}\frac{\tau^{(s)}_{\rm tr}}{\tau}\right)^2 G^R_s G^A_s, \tag{24}$$

where $\tau^{(s)}_{\rm tr}$ is the transport time in the subband s. Comparing with Eq. (17), we see that operator Γ has a matrix form similar to P, and the only modification is caused by the squared transport time.

In contrast to the quantum scattering rates, the transport rates in the branches are different. In order to calculate the transport times, we solve a system of equations for the velocity vertexes in the subbands, v^x_s:

$$v^x_s(\varphi) = v_F\cos\varphi + \sum_{s'=\pm}(1 - s'R)\left\langle\frac{1+ss'\cos\theta}{2}v^x_{s'}(\varphi')\right\rangle_{\varphi'}. \tag{25}$$

The solution is given by

$$v^x_s(\varphi) = v_F\cos\varphi\,\tau^s_{\rm tr}/\tau,$$

where [20]

$$\frac{\tau^\pm_{\rm tr}}{\tau} = 1 \mp R. \tag{26}$$

As a result, we obtain[1]

$$\sigma_{\rm bs}(B) = -\frac{e^2}{2\pi^2\hbar}(1+3R^2)\left(\frac{l}{l_B}\right)^2 \times \sum_{N=0}^{\infty}{\rm Tr}\left[\Pi A^3_N(\mathcal{I} - A_N)^{-1}\right], \tag{27}$$

[1]Strictly speaking, formally we get ${\rm Tr}[\Pi\bar{A}_N A^2_N(\mathcal{I} - A_N)^{-1}]$, where $\bar{A}_N$ is obtained from the matrix A_N by the substitution $R \to R(3+R^2)/(1+3R^2)$. However, replacing the matrix $\bar{A}_N$ by A_N does not change the trace.

where $\mathcal{I}$ is a 3×3 unit matrix, and

$$\Pi = \mathrm{diag}(1,-1,1). \tag{28}$$

The nonbackscattering contribution, given by a sum of the second diagram in Fig. 2 and the one conjugated to it, reads

$$\sigma_{\text{non-bs}} = \frac{\hbar}{\pi}\sum_{\alpha\beta}\int d\boldsymbol{r}\int d\boldsymbol{r}' \times \int d\boldsymbol{r}''[K(\boldsymbol{r},\boldsymbol{r}')\mathcal{C}(\boldsymbol{r}',\boldsymbol{r}'')K(\boldsymbol{r}'',\boldsymbol{r})]^{\alpha\beta}_{\beta\alpha}. \tag{29}$$

Here, the vertex is given by

$$K(\boldsymbol{r},\boldsymbol{r}') = \frac{iel}{\hbar}\sum_{s=\pm}\frac{\tau_{\text{tr}}^{(s)}}{\tau}V_0^2 G_s^R(\boldsymbol{r},\boldsymbol{r}')G_s^A(\boldsymbol{r},\boldsymbol{r}')\cos(\varphi-\varphi'), \tag{30}$$

where φ and φ' are polar angles of the vectors $\boldsymbol{r}$ and $\boldsymbol{r}'$, respectively. Summation over s yields

$$K(\boldsymbol{r},\boldsymbol{r}') = \frac{iel}{\hbar}\cos(\varphi-\varphi')(1+R^2)P(R'), \tag{31}$$

where the matrix $P(R')$ is given by P, Eq. (18), with R replaced by

$$R' = \frac{2R}{1+R^2}. \tag{32}$$

In the basis of Landau level states with charge $2e$ and fixed $N+s_z$, the operator $K(\boldsymbol{r},\boldsymbol{r}')$ is written as

$$K = \frac{1}{2}K_N^T - \frac{1}{2}K_{N+1}, \tag{33}$$

where the matrix K_N is

$$K_N = \begin{pmatrix} \frac{1}{2}P^{(1)}_{N-2} & -i\frac{R'}{\sqrt{2}}P^{(2)}_{N-2} & \frac{1}{2}P^{(3)}_{N-2} \\ i\frac{R'}{\sqrt{2}}P_{N-1} & P^{(1)}_{N-1} & i\frac{R'}{\sqrt{2}}P^{(2)}_{N-1} \\ -\frac{1}{2}P^{(1)}_{N-1} & -i\frac{R'}{\sqrt{2}}P_N & \frac{1}{2}P^{(1)}_N \end{pmatrix}. \tag{34}$$

Finally, we obtain

$$\sigma_{\text{non-bs}}(B) = \frac{e^2}{4\pi^2\hbar}(1+R^2)^2\left(\frac{l}{l_B}\right)^2 \times \sum_{N=0}^{\infty}\mathrm{Tr}\big[K_N\Pi K_N^T A_N(\mathcal{I}-A_N)^{-1} + K_N^T\Pi K_N A_{N+1}(\mathcal{I}-A_{N+1})^{-1}\big]. \tag{35}$$

B. Fermi level below the Dirac point

For the Fermi level below the Dirac point, $R>1$ in Fig. 1, the Green's functions for the two Fermi circles $i=1,2$ are different due to unequal values of the Fermi wave vectors $k_{\text{F}}^{(1,2)}$. Therefore, we have

$$P(\boldsymbol{r},\boldsymbol{r}') = V_0^2\sum_{i=1,2}G_i^R(\boldsymbol{r},\boldsymbol{r}')G_i^A(\boldsymbol{r},\boldsymbol{r}'). \tag{36}$$

The products $G_i^R G_i^A$ have the same coordinate dependence as at the Fermi level above the Dirac point; the difference is only in the density of states factors g_i, Eq. (12). As a result, $P(\boldsymbol{r},\boldsymbol{r}')$ has the same form as in a one-subband system with $s=-$ with the density of states equal to g_1+g_2. The conductivity correction in such a system is the same as in the single branch $s=-$ with $R=1$ and the transport time $\tau_{\text{tr}}=2\tau$. Therefore, the corrections σ_{bs} and $\sigma_{\text{non-bs}}$ are given by Eqs. (27) and (35) with $R=1$.

The above consideration shows that the conductivity correction at $R>1$ is equal to that at $R=1$. In other words, when the Fermi level goes down through the Dirac point at $k=0$, the correction does not change with further decreasing the Fermi energy to the bottom of the conduction band.

IV. RESULTS AND DISCUSSION

Let us now discuss the obtained expressions for the conductivity corrections. We remind the reader that Eqs. (27) and (35) have been obtained under the condition $|k_{\text{F}}^+ - k_{\text{F}}^-|l \gg 1$. At small Rashba splitting relative to the Fermi energy, $R\to 0$, the derived conductivity corrections coincide with the result obtained in Refs. [10,12] for weakly split spin subbands, $|k_{\text{F}}^+ - k_{\text{F}}^-| \ll k_{\text{F}}^+ + k_{\text{F}}^-$ in the limit of fast spin rotations $\Delta\tau/\hbar\to\infty$.

At the Fermi level lying exactly in the Dirac point, $R=1$, our results pass into the expressions obtained in Ref. [29] for the spectrum consisting of a single massless Dirac cone. A single-cone result for the considered two-subband system at $R=1$ follows from the zero density of states of the subband $s=+$ (the Fermi wave vector for it is equal to zero). In this case, the contribution of this subband to the conductivity is zero and scattering to it from the other branch is absent. Therefore, the subband $s=+$ is excluded from transport while the states in the other branch ($s=-$) are described by the same spinors as in a single valley of graphene or on the surface of a three-dimensional topological insulator. The same result is obtained for a single spin subband in a 2D topological insulator at the critical quantum well width (no gap) in Ref. [26] (this corresponds to $\eta=1$ there).

A. Zero-field conductivity correction

At zero field, the conductivity corrections are obtained from Eqs. (27) and (35) by passing to integration over N. This yields

$$\sigma_{\text{bs}}(B=0) = -\frac{e^2(1+3R^2)}{4\pi^2\hbar} \times \int_0^{1/(1+\gamma)}\frac{dP}{P^3}\mathrm{Tr}[\Pi A^3(\mathcal{I}-A)^{-1}], \tag{37}$$

$$\sigma_{\text{non-bs}}(B=0) = \frac{e^2}{8\pi^2\hbar}(1+R^2)^2 \times \int_0^{1/(1+\gamma)}\frac{dP}{P^3}\mathrm{Tr}[(K\Pi K^T + K^T\Pi K) \times A(\mathcal{I}-A)^{-1}]. \tag{38}$$

Here, the matrices A and K are obtained from A_N and K_N ($N\gg 1$) by substitutions [26,30]

$$P_N \approx \frac{1}{\sqrt{4N(l/l_B)^2+(1+\gamma)^2}} \equiv P, \qquad P_N^{(m)} \approx P\left[\frac{1-P(1+\gamma)}{1+P(1+\gamma)}\right]^{m/2}, \tag{39}$$

with $\gamma = \tau/\tau_\phi$. Note that P is expressed [31] as the Fourier transform with respect to $\boldsymbol{r} - \boldsymbol{r}'$ of the function $P_0(\boldsymbol{r},\boldsymbol{r}')$ defined in Eq. (19) with $\Phi(\boldsymbol{r},\boldsymbol{r}') = 0$. The corresponding wave vector is given by $q = 2N/l_B$.

Calculating the traces in Eqs. (37) and(38), we get

$$\sigma(B=0) = -\frac{e^2}{\pi^2\hbar}\int_0^{1/(1+\gamma)} dP \frac{\mathcal{K}(P,R,\gamma)}{[1-(1+\gamma)(R^2-1)P^3 - (2\gamma+2-R^2)P^2 + P\gamma](P\gamma+1)(1+P+P\gamma)^3}. \quad (40)$$

The explicit form of the function $\mathcal{K}(P,R,\gamma)$ is derived in the Supplemental Material [31]. When one is interested in the corrections up to $O(1)$ in the limit $\gamma \to 0$, γ in the numerator of Eq. (40) can be neglected, which yields

$$\begin{aligned}\mathcal{K}(P,R,0) = {} & (R^2-1)(3R^4+16R^2+9)P^4 \\ & + (10-5R^6+17R^2+6R^4)P^3 \\ & + (14+11R^2-6R^4+R^6)P^2 \\ & + (2-10R^4-5R^2+R^6)P - (1+3R^4).\end{aligned} \quad (41)$$

Furthermore, one can also neglect γ in the nonsingular factors in the denominator. For this reason, finding the roots of the cubic polynomial in the square brackets in the denominator of Eq. (40) perturbatively in $\gamma \ll 1$, we replace it by

$$[1+P-P^2(1-R^2)]\left(1-P-\gamma\frac{R^2}{1+R^2}\right). \quad (42)$$

Then, integration in Eq. (40) yields

$$\sigma(B=0) = \sigma_{\rm diff}(T) + \sigma_{\rm ball}(R). \quad (43)$$

The first term here is the diffusive contribution dependent on the temperature T via τ_ϕ:

$$\sigma_{\rm diff}(T) = \frac{e^2}{4\pi^2\hbar}\ln\left[\frac{\tau_\phi(T)}{\tau}\right]. \quad (44)$$

We emphasize that the coefficient in front of the logarithm is independent of R. It is worth stressing that the coefficients in divergent logarithmic terms related to both backscattering and nonbackscattering contributions are R dependent [31], and only the sum of these terms gives the universal coefficient $e^2/(4\pi^2\hbar)$ prescribed by a symplectic class of symmetry.

It is shown in Appendix C that, in the experimentally relevant case of fixed electron concentration, the dephasing time τ_ϕ is independent of R, so that the argument of the logarithm in Eq. (44) also does not depend on R. The dependence on R, however, appears in the ballistic term which takes into account the interference corrections from ballistic trajectories with a few (three or more, because we discuss the contribution sensitive to magnetic field) scattering events and is regular at low temperatures $\tau/\tau_\phi \ll 1$. At $\tau/\tau_\phi = 0$ we obtain the following analytical expression for the ballistic contribution to the conductivity correction:

$$\begin{aligned}\sigma_{\rm ball}(R) = -\frac{e^2}{4\pi^2\hbar}\Bigg\{ & \frac{3+8R^2+R^4}{4} - \frac{4-R^2(1+R^2)}{2}\ln 2 \\ & - \frac{2+R^2+R^4}{4}\ln(1+R^2) \\ & + \frac{8-13R^2+5R^4}{2\sqrt{5-4R^2}}\ln\frac{3+\sqrt{5-4R^2}}{2\sqrt{1+R^2}}\Bigg\}.\end{aligned} \quad (45)$$

In particular, we find

$$\sigma_{\rm ball}(R) = -\frac{e^2}{4\pi^2\hbar}\begin{cases} 3/4 - 2\ln 2 + \frac{4}{\sqrt{5}}\ln\frac{3+\sqrt{5}}{2}, & R=0, \\ 3-2\ln 2, & R=1, \end{cases} \quad (46)$$

which gives the values $-0.0275e^2/\hbar$ at $R=0$ and $-0.041e^2/\hbar$ at $R=1$.

The correction $\sigma_{\rm ball}(R)$ determines the dependence of the total conductivity correction on the spin-orbit splitting. The zero-field conductivity correction is presented in Fig. 3. In contrast to the result of the diffusion approximation, the total correction depends, however, on the Fermi level position at $0 < R < 1$. The correction saturates at a certain value after the Fermi level crosses the Dirac point, at $R \geqslant 1$ (see Sec. III B). A significant difference between the exact result and the result obtained within the diffusive approximation, Eq. (44), which is clearly seen in Fig. 3, demonstrates the essential role of ballistic processes in weak localization at realistic values of τ/τ_ϕ.

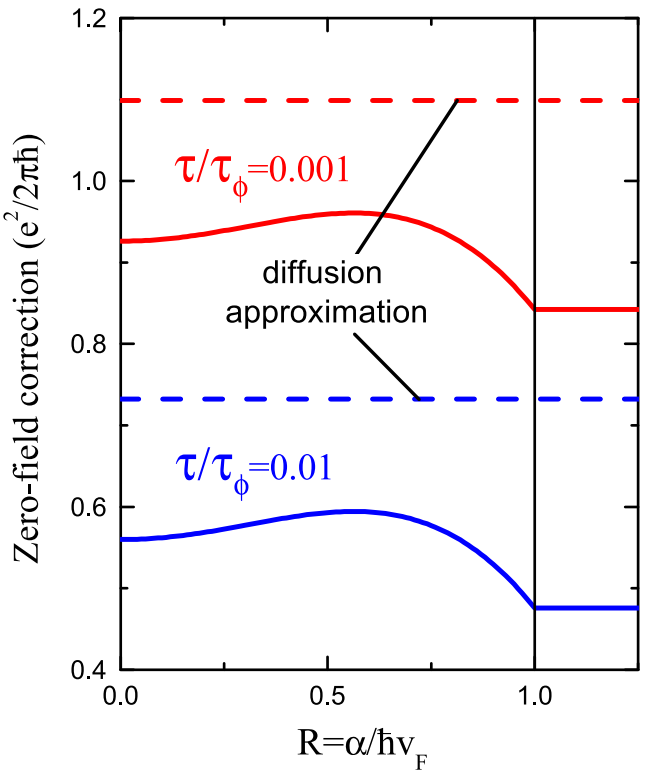

FIG. 3. Zero-field conductivity correction as a function of the Rashba splitting parameter $R = \alpha/(\hbar v_{\rm F})$ (solid curves). The diffusive contribution to the quantum correction, Eq. (44), is independent of R (dashed curves).

For a system of a finite size L the conductivity correction is finite even in the absence of dephasing. At $\gamma = 0$ we integrate in Eq. (40) up to $P = 1 - l^2/(2L^2)$ and obtain

$$\sigma_L(R) = \frac{e^2}{4\pi^2\hbar} \ln\frac{2L^2}{l^2} - \frac{e^2}{4\pi^2\hbar} \ln(1+R^2) + \sigma_{\rm ball}(R). \quad (47)$$

This equation shows that the ballistic correction calculated without dephasing, when the diffusive contribution is cut off by the system size, differs from the result calculated at finite dephasing by the term $\propto \ln(1+R^2)$. This is related to the fact that τ_ϕ/τ corresponds to $L^2/(D\tau)$ in the logarithmic diffusive contribution, where $D = (1+R^2)l^2/(2\tau)$ is the diffusion coefficient (see Appendix A).

As discussed above, the zero-field correction can be also obtained by calculations in the momentum space in the basis of chiral subband states (3). This alternative derivation, leading to the same results, is presented in Appendix B and the Supplemental Material [31]. Backscattering and nonbackscattering contributions to the conductivity correction are calculated and their dependences on R and on the dephasing rate are analyzed. It is shown in the Supplemental Material [31] that the backscattering and the nonbackscattering contributions to the conductivity have the same order of magnitude and different signs compensating each other to a large extent.

B. Magnetoconductivity

The magnetic field dependence of the conductivity correction is given by Eqs. (27) and (35). The results of calculations are shown in Fig. 4. The magnetic field is given in units of the characteristic field B_0,

$$B_0 = \frac{\hbar}{|e|l^2}. \quad (48)$$

The correction monotonously decreases with the magnetic field for all R. The magnetoconductivity varies with the Rashba splitting. The magnetic field dependence is stronger at $R \approx 0.5$ due to the higher zero-field value of the correction (see Fig. 3). The magnetic field dependencies at a given R coincide in fields $B \gtrsim 0.1B_0$ independently of the value of τ_ϕ/τ. The reason is that the magnetic-field-induced phase which breaks the interference is stronger in those fields than dephasing.

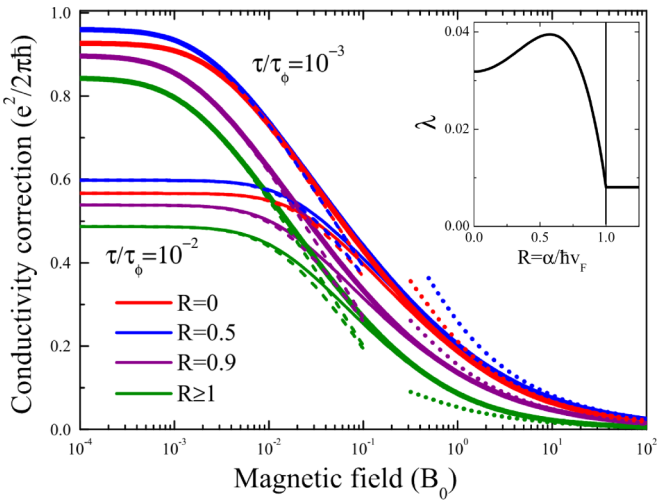

FIG. 4. Magnetoconductivity at different $R = \alpha/(\hbar v_F)$. The dephasing rate $\tau/\tau_\phi = 10^{-2}$ (thin solid curves) and $\tau/\tau_\phi = 10^{-3}$ (thick solid curves). Dashed lines present the diffusion approximation results, Eq. (54). Dotted lines are high-field asymptotics, Eq. (49). The inset shows the function $\lambda(R)$, Eq. (53), describing the high-field asymptotics of the conductivity correction.

In high magnetic fields $B \gg B_0$ (but still B is classically weak), the conductivity correction decreases according to the following asymptotic law:

$$\sigma_{\rm hf} = \frac{e^2}{\hbar}\lambda(R)\sqrt{\frac{B_0}{B}}. \quad (49)$$

The function $\lambda(R)$ is a sum of backscattering and nonbackscattering contributions, $\lambda = \lambda_{\rm bs} + \lambda_{\text{non-bs}}$, where

$$\lambda_{\rm bs} = -\frac{1+3R^2}{2\pi^2}\sum_{N=0}^{\infty} {\rm Tr}\big(\Pi\tilde{A}_N^3\big), \quad (50)$$

$$\lambda_{\text{non-bs}} = \frac{(1+R^2)^2}{4\pi^2} \times \sum_{N=0}^{\infty} {\rm Tr}\big(\tilde{K}_N\Pi\tilde{K}_N^T\tilde{A}_N + \tilde{K}_N^T\Pi\tilde{K}_N\tilde{A}_{N+1}\big). \quad (51)$$

The matrices $\tilde{A}_N$ and $\tilde{K}_N$ are obtained from A_N and K_N by the following substitutions [26]: All $P_N^{(m)}$ with odd N should be taken by zeros, and at even $N = 2k$,

$$P_{2k} \to \sqrt{\frac{\pi}{2}}\frac{(2k)!}{2^{2k}(k!)^2}, \quad P_{2k}^{(2)} \to \sqrt{\frac{\pi}{2}}\frac{\sqrt{(2k)!(2k+2)!}}{2^{2k+1}k!(k+1)!},$$
$$P_{2k}^{(1)} \to -\frac{1}{\sqrt{2k+1}}, \quad P_{2k}^{(3)} \to -\sqrt{\frac{2k+2}{(2k+1)(2k+3)}}. \quad (52)$$

From Eqs. (50)–(52) we obtain

$$\lambda(R) = \frac{\sqrt{\pi}(5R^2+3)}{32\sqrt{2}\Gamma^4(3/4)} - \frac{45R^4+26R^2+13}{256\sqrt{2\pi}}. \quad (53)$$

The dependence $\lambda(R)$ is shown in the inset to Fig. 4. The high-field asymptotes Eq. (49) are presented in Fig. 4 by the dotted lines.

A comparison with the results of the exact calculation shows that the asymptotes perfectly describe the conductivity correction at $B \gtrsim 10B_0$, but only the exact expressions describe the magnetoconductivity in the intermediate range of fields.

The magnetoconductivity $\delta\sigma(B) = \sigma(B) - \sigma(0)$ in the diffusion approximation is given by the conventional expression for systems with fast spin relaxation,

$$\delta\sigma_{\rm diff}(B) = -\frac{e^2}{4\pi^2\hbar}[\psi(1/2+1/b) + \ln b],$$
$$b = 2\frac{B}{B_0}\frac{\tau_\phi}{\tau}(1+R^2) = \frac{4D\tau_\phi}{l_B^2}, \quad (54)$$

where $\psi(x)$ is digamma function. The dependences $\sigma(0) + \delta\sigma_{\rm diff}(B)$ with $\sigma(0)$ calculated by Eqs. (43)–(45) are plotted in Fig. 4 by dashed lines. It is well known that the diffusion approximation does not describe the magnetoconductivity in fields $B \gtrsim B_0$ [10,29]. Our calculation demonstrates that diffusion approximation satisfactorily describes the

magnetic field dependence of the conductivity correction up to $(0.02\ldots0.03)B_0$ (see Fig. 4).

Figure 4 demonstrates that neither the diffusion approximation nor high-field asymptotics describe the conductivity correction, and the exact expressions are needed to describe the magnetic field dependence in the whole range of classically weak fields.

V. CONCLUSION

In this work we have developed the theory of weak localization in 2D systems with an arbitrary strong linear-in-$\boldsymbol{k}$ spin-orbit splitting of the energy spectrum. The theory describes weak antilocalization in systems with the Rashba or Dresselhaus isotropic spin-orbit splittings. We have derived an analytical expression for the conductivity correction that includes both diffusive and ballistic contributions and is valid in a wide interval of phase breaking rates and magnetic fields. We have found that the ballistic contribution depends solely on the spectrum characteristics [see Eq. (45)] and, therefore, reflects the intrinsic properties of the system. We have also shown that the magnetoconductivity varies with the Fermi energy when the Fermi level is above the "Dirac point" of the spectrum, but does not depend on the Fermi energy when it goes below this point.

ACKNOWLEDGMENTS

We thank M. O. Nestoklon for helpful discussions. Partial financial support from the Russian Foundation for Basic Research, the EU Network FP7-PEOPLE-2013-IRSES Grant No. 612624 "InterNoM," by Programmes of RAS, and DFG-SPP1666 is gratefully acknowledged.

APPENDIX A: DRUDE CONDUCTIVITY

Although the Drude conductivity in a system with well-separated spin branches has been calculated in Ref. [20], we rederive it in this Appendix, in order to introduce the kinetic equation with quantum corrections that lead to the interference contribution to the conductivity (see Appendix B below).

The distribution function of electrons with energy $E = E_F$ in the two-band model can be written as

$$f = \sum_{s=\pm} A_s(\varphi)\delta[E_F - E_s(k)], \tag{A1}$$

so that the current reads

$$j_x = ev_F \sum_{s=\pm} g_s \langle A_s(\varphi)\cos\varphi\rangle_\varphi. \tag{A2}$$

Here, v_F is the Fermi velocity, Eq. (5), equal in both branches, the angular brackets denote averaging over φ, and the densities of states at the Fermi energy in the branches are given by Eq. (8).

Within the Drude-Boltzmann approximation, functions $A_s(\varphi)$ obey the system of two coupled balance equations:

$$-e\mathcal{E}v_F\cos\varphi = \sum_{s'=\pm}\left\langle \Gamma^{\rm in}_{ss'}(\varphi-\varphi')A_{s'}(\varphi') - \Gamma^{\rm out}_{s's}(\varphi-\varphi')A_s(\varphi)\right\rangle_{\varphi'}. \tag{A3}$$

Here, $\mathcal{E}$ is the electric field, and we have introduced the ingoing and outgoing scattering rates,

$$\Gamma^{\rm in}_{ss'}(\theta) = \frac{2\pi}{\hbar}|V_{ss'}(\theta)|^2 g_{s'}, \quad \Gamma^{\rm out}_{ss'}(\theta) = \frac{2\pi}{\hbar}|V_{ss'}(\theta)|^2 g_s, \tag{A4}$$

which are related as follows: $\Gamma^{\rm in}_{ss'} = \Gamma^{\rm out}_{s's}$. The total outgoing rates, Eq. (7), coincide for two bands,

$$\frac{1}{\tau} = \langle\Gamma^{\rm out}_{++} + \Gamma^{\rm out}_{-+}\rangle_\theta = \langle\Gamma^{\rm out}_{--} + \Gamma^{\rm out}_{+-}\rangle_\theta = \frac{2\pi}{\hbar}\frac{g_+ + g_-}{2}|V_0|^2. \tag{A5}$$

We search for solution of Eq. (A3) in the form

$$A_s = a_s e\mathcal{E}l\cos\varphi, \tag{A6}$$

where a_s are dimensionless coefficients. In terms of a_s the Drude conductivity reads

$$\sigma_D = \frac{e^2 v_F^2 \tau}{2}\sum_{s=\pm} g_s a_s. \tag{A7}$$

Substituting Eq. (A6) into Eq. (A3), we see that a_s obey the following set of coupled equations,

$$1 = a_s - \sum_{s'}\gamma_{ss'}a_{s'}, \tag{A8}$$

where

$$\gamma_{ss'} = \tau\left\langle\Gamma^{\rm in}_{ss'}(\theta)\cos\theta\right\rangle_\theta. \tag{A9}$$

Simple calculation yields

$$\gamma_{++} = -\gamma_{-+} = \frac{g_+}{2(g_+ + g_-)}, \qquad \gamma_{--} = -\gamma_{+-} = \frac{g_-}{2(g_+ + g_-)}, \tag{A10}$$

and

$$a_s = \frac{2g_s}{g_+ + g_-}. \tag{A11}$$

Finally, the Drude conductivity becomes

$$\sigma_D = e^2 v_F^2 \tau\frac{g_+^2 + g_-^2}{g_+ + g_-} = e^2 v_F^2 \tau\frac{m}{2\pi\hbar^2}(1+R^2). \tag{A12}$$

We note that for the fixed value of E_F, the Fermi velocity depends on R as

$$v_F^2 = \frac{2E_F}{m}\frac{1}{1-R^2}. \tag{A13}$$

As a result, we get

$$\sigma_D|_{E_F=\rm const} = \frac{e^2}{\pi}E_F\tau\frac{1+R^2}{1-R^2}. \tag{A14}$$

In fact, experimentally, it is the electron concentration that is fixed. When the Fermi level is located above the Dirac point, the electron concentration is given by

$$n = \frac{(k_F^+)^2 + (k_F^-)^2}{4\pi} = \frac{m}{\pi\hbar^2}\left(E_F + \frac{m\alpha^2}{\hbar^2}\right), \tag{A15}$$

where the Fermi wave vectors in the subbands are given by Eq. (4).

From Eq. (5) we express the Fermi velocity in terms of the fixed concentration and the parameter R:

$$v_F^2 = \frac{2\pi\hbar^2 n}{m^2(1+R^2)}. \tag{A16}$$

As a result, the Drude conductivity for a fixed value of n takes its conventional form:

$$\sigma_D = \frac{e^2 n\tau}{m}. \tag{A17}$$

Thus, the Drude conductivity for fixed electron concentration does not depend on R.

Writing the diffusion equations for 2D concentrations in two subbands, $n_\pm$, and noting that they are related as $n_+/n_- = g_+/g_-$, we obtain that the diffusion coefficient is also R independent for fixed n:

$$D = \frac{v_F^2\tau}{2}(1+R^2) = \frac{\pi\hbar^2 n\tau}{m^2}. \tag{A18}$$

APPENDIX B: QUANTUM CORRECTIONS TO KINETIC EQUATION

As it was shown in Ref. [9], the weak-localization correction to the conductivity can be interpreted in terms of localization-induced correction to scattering cross section on a single impurity. Below, we generalize this approach for the system with a strong Rashba splitting of the spectrum. The corresponding trajectories are presented in Fig. 5.

Within the kinetic equation formalism, weak localization leads to corrections to the ingoing scattering rates, so that Eq. (A8) modifies

$$1 = a_s - \sum_{s'}(\gamma_{ss'} + \delta\gamma_{ss'})a_{s'}, \quad s = \pm. \tag{B1}$$

Here, $\gamma_{ss'}$ are given by Eq. (A10),

$$\delta\gamma_{ss'} = \tau\left\langle \delta\Gamma^{\rm in}_{ss'}(\varphi)\cos\varphi\right\rangle_\varphi, \tag{B2}$$

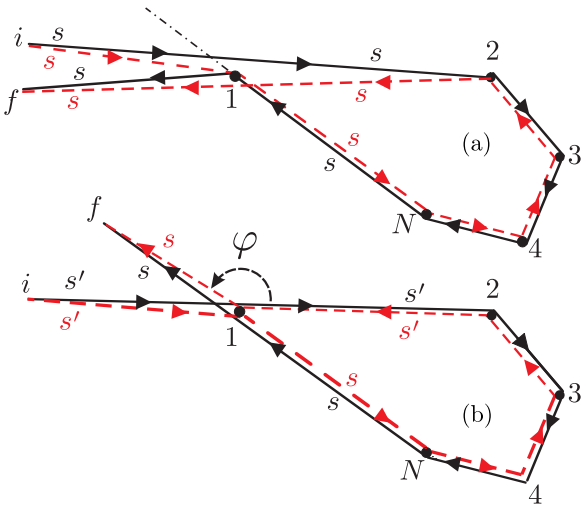

FIG. 5. Trajectories with N impurities giving rise to the quantum conductivity correction. The processes of backscattering (a) and scattering by an arbitrary angle φ (b) contribute to $\sigma_{\rm bs}$ and $\sigma_{\text{non-bs}}$, respectively.

and $\delta\Gamma^{\rm in}_{ss'}$ are the interference-induced corrections to the scattering rates. Treating the correction $\delta\gamma_{ss'}a_{s'}$ as a small perturbation, one can replace in this term coefficients a_s with their Drude values given by Eq. (A11). Doing so, we find that the weak-localization-induced corrections to a_s obey

$$\begin{aligned}\lambda_+ &= \delta a_+ + \frac{g_-\delta a_- - g_+\delta a_+}{2(g_+ + g_-)},\\ \lambda_- &= \delta a_- + \frac{g_+\delta a_+ - g_-\delta a_-}{2(g_+ + g_-)},\end{aligned} \tag{B3}$$

where

$$\lambda_s = \frac{2}{g_+ + g_-}\sum_{s'}\delta\gamma_{ss'}g_{s'}. \tag{B4}$$

The conductivity correction is proportional to $\sum_s g_s\delta a_s$. Solving Eq. (B3), we get

$$\sum_s g_s\delta a_s = \frac{2}{g_+ + g_-}\sum_s \lambda_s g_s^2. \tag{B5}$$

Substituting Eq. (B5) into Eq. (A7) we express the conductivity correction via corrections to the scattering rates,

$$\sigma(B=0) = \frac{2e^2l^2}{(g_+ + g_-)^2}\sum_{ss'} g_s^2 g_{s'}\left\langle \delta\Gamma^{\rm in}_{ss'}(\varphi)\cos\varphi\right\rangle. \tag{B6}$$

Similar to Refs. [9,26], we express $\delta\Gamma^{\rm in}_{ss'}(\varphi)$ in terms of return probability $w_{ss'}(\varphi)$, which depends now on the branch indices (s' initial branch, s final branch). To this end, we introduce the rates

$$\nu_{ss'}(\varphi) = l^2 w_{ss'}(\varphi) g_{s'} V^2_{s's}(\pi+\varphi) \tag{B7}$$

(rule of summation over repeated indices does not apply here). Correction $\delta\Gamma^{\rm in}_{ss'}(\varphi)$ is given by the sum of so-called backscattering and nonbackscattering corrections [9,26],

$$\delta\Gamma^{\rm in}_{ss'}(\varphi) = C_0\left[2\pi\delta_{ss'}\delta(\varphi-\pi)\sum_{s''}\langle\nu_{ss''}(\varphi')\rangle_{\varphi'} - \nu_{ss'}(\varphi)\right] \tag{B8}$$

with

$$C_0 = \frac{8\pi^2\hbar}{m v_F l}. \tag{B9}$$

This coefficient is responsible for the smallness of the quantum correction.

Substituting Eq. (B8) into Eq. (B6) and using $w_{ss'} = w_{s's}$ and $W_{ss'} = W_{s's}$, we finally get

$$\begin{aligned}\sigma(B=0) = -\frac{e^2l^2C_0}{4g_0^2}\Bigg\langle \sum_{ss'} g_s g_{s'}\big(g_s^2 + g_{s'}^2 \\ + 2g_s g_{s'}\cos\varphi\big)w_{ss'}(\varphi)V^2_{s's}(\pi+\varphi)\Bigg\rangle_\varphi.\end{aligned} \tag{B10}$$

This expression can be shown to coincide with a sum of Eqs. (37) and (38) of the main text (see also the Supplemental Material [31]).

APPENDIX C: DEPHASING DUE TO COULOMB INTERACTION

The equation for the cooperon in the presence of inelastic electron-electron scattering due to the Coulomb repulsion [1] reads (see the Supplemental Material [31])

$$\mathbf{C}_{ss'}(\varphi,\varphi';\boldsymbol{q}) = \mathbf{C}^0_{ss'}(\varphi,\varphi';\boldsymbol{q}) + \sum_{s_1 s_2} \int \frac{d\varphi_1}{2\pi} \int \frac{d\varphi_2}{2\pi} \mathbf{C}^0_{ss_1}(\varphi,\varphi_1;\boldsymbol{q}) \Sigma^{\phi}_{s_1 s_2}(\varphi_1,\varphi_2,\boldsymbol{q}) \mathbf{C}_{s_2 s'}(\varphi_2,\varphi';\boldsymbol{q}). \tag{C1}$$

The cooperon self-energy is, in general, a matrix in subband space, given by

$$\Sigma^{\phi}_{s_1 s_2}(\varphi_1,\varphi_2) = 16\pi^2\tau^4 g_{s_1} g_{s_2} \int_{-T}^{T} \frac{d\Omega}{(2\pi)} \int \frac{d^2Q}{(2\pi)^2} \frac{T}{\Omega} \mathrm{Im}\, U(\Omega,\boldsymbol{Q}) \mathbf{C}^0_{s_1 s_2}(\varphi_1,\varphi_2;\Omega,\boldsymbol{Q}) P(\varphi_1;\Omega,\boldsymbol{Q}) P(\varphi_2;\Omega,\boldsymbol{Q}). \tag{C2}$$

Here,

$$U(\Omega,\boldsymbol{Q}) = \frac{1}{2g_0} \frac{\mathrm{D}Q^2 - i\Omega}{\mathrm{D}Q^2}$$

is the Fourier component of the dynamically screened Coulomb potential [31], D is the diffusion coefficient, Eq. (A18), and $g_0 = m/(2\pi)$.

The integral over Ω diverges logarithmically at $\Omega \to 0$. We regularize this divergence self-consistently in a usual way [1] at Ω of the order of the dephasing rate $1/\tau_\phi$ and get

$$\Sigma^{\phi}_{s_1 s_2} \simeq -e^{i(\varphi_2-\varphi_1)} \frac{s_1 s_2 g_{s_1} g_{s_2}}{g_0} \frac{\pi\tau^2}{\tau_\phi}, \tag{C3}$$

with

$$\frac{1}{\tau_\phi} = \frac{T}{4\pi g_0 \mathrm{D}} \ln(T\tau_\phi) \simeq \frac{T}{4\pi g_0 \mathrm{D}} \ln(4\pi g_0 \mathrm{D}). \tag{C4}$$

In the diffusion approximation $ql \ll 1$, the solution of Eq (C1) with the self-energy (C3) takes the form [31]

$$\mathbf{C}_{ss'}(\varphi,\varphi';\boldsymbol{q}) \simeq \frac{e^{i(\varphi'-\varphi)}}{4\pi g_0 \tau^2} \left\{ \frac{ss' + iqlR(s'\cos\varphi + s\cos\varphi')}{\mathrm{D}q^2 + \frac{1}{\tau_\phi}} + 2\tau \left[\sin\varphi \sin\varphi' + \frac{\frac{\mathrm{D}}{1+R^2}q^2 + \frac{1}{\tau_\phi}}{\mathrm{D}q^2 + \frac{1}{\tau_\phi}} \cos\varphi \cos\varphi' \right] \right\}. \tag{C5}$$

The logarithmically divergent diffusive term in the conductivity correction is thus cut off by $1/\tau_\phi$ given by Eq. (C4).

In the experimentally relevant case, when the electron concentration n is kept fixed by applying the gate voltage, the diffusion coefficient D (and hence the ratio τ_ϕ/τ) do not depend on R [see Eqs. (A18) and (C4)]:

$$\frac{\tau}{\tau_\phi} = \frac{mT}{2\pi n} \ln \frac{2\pi n\tau}{m}. \tag{C6}$$

As a result, the T-dependent diffusive term Eq. (44),

$$\sigma_{\mathrm{diff}}(T) = \frac{e^2}{4\pi^2\hbar} \ln \frac{\tau_\phi}{\tau} \simeq \frac{e^2}{4\pi^2\hbar} \ln \frac{2\pi\hbar^2 n}{mT \ln(2\pi\hbar n\tau/m)}, \tag{C7}$$

is R independent for fixed n.

[1] B. L. Altshuler and A. G. Aronov, in *Electron-Electron Interactions in Disordered Systems*, edited by A. L. Efros and M. Pollak (Elsevier, Amsterdam, 1985).

[2] G. Bergmann, Phys. Rep. **107**, 1 (1984).

[3] V. F. Gantmakher, *Electrons and Disorder in Solids*, translated by L. I. Man, International Series of Monographs on Physics Vol. 130 (Oxford University Press, Oxford, U.K., 2005).

[4] S. V. Iordanskii, Yu. B. Lyanda-Geller, and G. E. Pikus, Pisma Zh. Eksp. Teor. Fiz. **60**, 199 (1994) [JETP Lett. **60**, 206 (1994)].

[5] W. Knap, C. Skierbiszewski, A. Zduniak, E. Litwin-Staszewska, D. Bertho, F. Kobbi, J. L. Robert, G. E. Pikus, F. G. Pikus, S. V. Iordanskii, V. Mosser, K. Zekentes, and Yu. B. Lyanda-Geller, Phys. Rev. B **53**, 3912 (1996).

[6] G. M. Minkov, A. V. Germanenko, O. E. Rut, A. A. Sherstobitov, L. E. Golub, B. N. Zvonkov, and M. Willander, Phys. Rev. B **70**, 155323 (2004).

[7] V. M. Gasparyan and A. Yu. Zyuzin, Fiz. Tverd. Tela (Leningrad) **27**, 1662 (1985) [Sov. Phys. Solid State **27**, 999 (1985)].

[8] M. I. Dyakonov, Solid State Commun. **92**, 711 (1994).

[9] A. P. Dmitriev, V. Yu. Kachorovskii, and I. V. Gornyi, Phys. Rev. B **56**, 9910 (1997).

[10] L. E. Golub, Phys. Rev. B **71**, 235310 (2005).

[11] M. M. Glazov and L. E. Golub, Semiconductors **40**, 1209 (2006).

[12] M. M. Glazov and L. E. Golub, Semicond. Sci. Technol. **24**, 064007 (2009).

[13] S. McPhail, C. E. Yasin, A. R. Hamilton, M. Y. Simmons, E. H. Linfield, M. Pepper, and D. A. Ritchie, Phys. Rev. B **70**, 245311 (2004).
[14] D. Spirito, L. Di Gaspare, F. Evangelisti, A. Di Gaspare, E. Giovine, and A. Notargiacomo, Phys. Rev. B **85**, 235314 (2012).
[15] I. S. Lyubinskiy and V. Yu. Kachorovskii, Phys. Rev. B **70**, 205335 (2004); Phys. Rev. Lett. **94**, 076406 (2005).
[16] S. D. Ganichev and L. E. Golub, Phys. Status Solidi B **251**, 1801 (2014).
[17] M. Sakano, M. S. Bahramy, A. Katayama, T. Shimojima, H. Murakawa, Y. Kaneko, W. Malaeb, S. Shin, K. Ono, H. Kumigashira, R. Arita, N. Nagaosa, H. Y. Hwang, Y. Tokura, and K. Ishizaka, Phys. Rev. Lett. **110**, 107204 (2013).
[18] H. Liang, L. Cheng, L. Wei, Z. Luo, G. Yu, C. Zeng, and Z. Zhang, Phys. Rev. B **92**, 075309 (2015).
[19] G. M. Minkov, A. V. Germanenko, O. E. Rut, A. A. Sherstobitov, S. A. Dvoretski, and N. N. Mikhailov, Phys. Rev. B **89**, 165311 (2014).
[20] V. Brosco, L. Benfatto, E. Cappelluti, and C. Grimaldi, Phys. Rev. Lett. **116**, 166602 (2016).
[21] I. V. Gornyi, A. P. Dmitriev, and V. Yu. Kachorovskii, JETP Lett. **68**, 338 (1998).
[22] M. A. Skvortsov, JETP Lett. **67**, 133 (1998).
[23] G. Tkachov and E. M. Hankiewicz, Phys. Rev. B **84**, 035444 (2011).
[24] V. Krueckl and K. Richter, Semicond. Sci. Technol. **27**, 124006 (2012).
[25] P. M. Ostrovsky, I. V. Gornyi, and A. D. Mirlin, Phys. Rev. B **86**, 125323 (2012).
[26] I. V. Gornyi, V. Yu. Kachorovskii, and P. M. Ostrovsky, Phys. Rev. B **90**, 085401 (2014).
[27] I. V. Gornyi, V. Yu. Kachorovskii, A. D. Mirlin, and P. M. Ostrovsky, Phys. Status Solidi B **251**, 1786 (2014).
[28] M. I. Dyakonov and V. Yu. Kachorovskii, Fiz. Tekh. Poluprovodn. **20**, 178 (1986) [Sov. Phys. Semicond. **20**, 110 (1986)].
[29] M. O. Nestoklon, N. S. Averkiev, and S. A. Tarasenko, Solid State Commun. **151**, 1550 (2011).
[30] M. O. Nestoklon and N. S. Averkiev, Phys. Rev. B **90**, 155412 (2014).
[31] See Supplemental Material at http://link.aps.org/supplemental/10.1103/PhysRevB.93.245306 for technical details.